# Evidence for electronic gap-driven metal-semiconductor transition in phase-change materials

Dmitry Shakhvorostov[a], Razvan A. Nistor[a], Lia Krusin-Elbaum[b,1], Glenn J. Martyna[b], Dennis M. Newns[b], Bruce G. Elmegreen[b], Xiao-hu Liu[b], Zak E. Hughes[a], Sujata Paul[b], Cyril Cabral[b], Simone Raoux[c], David B. Shrekenhamer[d], Dimitri N. Basov[d], Young Song[e], and Martin H. Müser[a]

[a]Department of Applied Mathematics, University of Western Ontario, London, ON, Canada N6A5B7; [b]IBM T. J. Watson Research Center, Yorktown Heights, NY 10598; [c]IBM Almaden Research Center, San Jose, CA 95120; [d]Physics Department, University of California at San Diego, La Jolla, CA 92093; and [e]Department of Chemistry, University of Western Ontario, London, ON, Canada N6A5B7

Edited by Mildred S. Dresselhaus, Massachusetts Institute of Technology, Cambridge, MA, and approved May 12, 2009 (received for review December 19, 2008)

**Phase-change materials are functionally important materials that can be thermally interconverted between metallic (crystalline) and semiconducting (amorphous) phases on a very short time scale. Although the interconversion appears to involve a change in local atomic coordination numbers, the electronic basis for this process is still unclear. Here, we demonstrate that in a nearly vacancy-free binary GeSb system where we can drive the phase change both thermally and, as we discover, by pressure, the transformation into the amorphous phase is electronic in origin. Correlations between conductivity, total system energy, and local atomic coordination revealed by experiments and long time ab initio simulations show that the structural reorganization into the amorphous state is driven by opening of an energy gap in the electronic density of states. The electronic driving force behind the phase change has the potential to change the interconversion paradigm in this material class.**

ab initio simulations | structural phase change | electronic phase transitions | ac conductivity

Metal–semiconductor transitions in condensed matter often occur concurrently with structural transformations. There is a longstanding and much debated issue as to whether the driving force in these transitions is fundamentally electronic or structural in origin (1). This problem is particularly challenging in cases where the semiconducting phase is a glassy one, as in the class of the technologically important phase-change materials (2–4). These are typically alloys of Ge, Sb, and Te, which in certain composition ranges, such as a canonical compound $Ge_2Sb_2Te_5$ (225), can be converted between the conducting crystalline phase and a semiconducting amorphous phase. The considerable body of work on these materials (5) has made it clear that conversion to the amorphous state involves a change in local coordination number resembling an "umbrella flip" (4) in some members of the class. But, the 2 key fundamental questions, why the system would turn semiconducting on executing this local structural rearrangement and what is the driving force behind this process, still remain unanswered.

The difficulty in following the causal linkage between electronic and atomistic configurations during the phase transition (6, 7) lies in part in the short time scales of the process (4, 8), in part, in the nonequilibrium (nonergodic) nature of the glassy amorphous states (9), and, in part, in the global nature of the usual experimental techniques, such as charge transport or optical reflectivity (3). Electronic driving mechanisms for the phase-change considered early on (2, 10) were never satisfactorily proved (11), whereas numerous ab initio molecular dynamics (MD) studies (12–15) tended to emphasize local atomic rearrangements (16) while sidelining the relationship to electronic structure.

Here, we demonstrate the causal link between the atomic and electronic structure during the phase change by choosing a very simple binary compound GeSb, having 2 critically important advantages. First, it is nearly vacancy free. Unlike the complex ternary $Ge_2Sb_2Te_5$ (225) that has a large number of vacancies (17) (the 225 lattice is a 2-site NaCl type, with Te on the Cl sublattice and Ge + Sb + vacancy on the Na sublattice), GeSb has only 1 (Sb) lattice with Ge substituting on the Sb sites. This is critical because during the phase-change process, along with the (orders of magnitude) jump in resistivity (3), there is a volume (density) change. The GeSb amorphous state is ≈8% less dense than the crystalline form (18), so, by Le Chatelier's principle, applying pressure (decreasing volume) should induce a change from the amorphous to the crystalline form. This will give us an isothermal path to induce the phase change.

We note that pressure-induced crystallization of GeSb has no analog in the 225 material. Instead, under pressure, there is the contrary phenomenon of amorphization (19). This process is clearly controlled by the high vacancy concentration intrinsic to the 225 crystal structure, where pressure then acts to "squeeze out" these vacancies, irreversibly denaturing the crystalline 225.

Second, the crystallization velocity in GeSb is very high (8). This—in addition to the isothermal means of reaching the amorphous state being simpler—significantly reduces the demand on computational resources (12, 14) required to track the process by using ab initio MD (AIMD) and to test the MD results against our experimental data.

Our principal finding is that the process of structural reorganization is driven by opening of the electronic gap, so that the end stage of the amorphization process is a fully gapped system, i.e., a semiconductor. The existence of an electronic driving force behind the phase change has a potential to alter future technological embodiments of this material class.

## Results and Discussion

We focus on the eutectic composition (15 atm % Ge), which has a robust amorphous phase (20) and large amorphous/crystalline resistance ratio (see Fig. 1*A*). It crystallizes exothermally at

Author contributions: L.K.-E., D.M.N., G.J.M., and M.H.M. designed research; D.S., R.A.N., L.K.-E., G.J.M., D.M.N., B.G.E., X.-h.L., Z.E.H., S.P., C.C., D.B.S., D.N.B., Y.S., and M.H.M. performed research; S.R. and Y.S. contributed new reagents/analytic tools; L.K.-E., D.M.N., G.J.M., and M.H.M. analyzed data; and L.K.-E., D.M.N., G.J.M., and M.H.M. wrote the paper.

The authors declare no conflict of interest.

This article is a PNAS Direct Submission.

Freely available online through the PNAS open access option.

To whom correspondence should be addressed. E-mail: krusin@us.ibm.com.

This article contains supporting information online at www.pnas.org/cgi/content/full/0812942106/DCSupplemental.

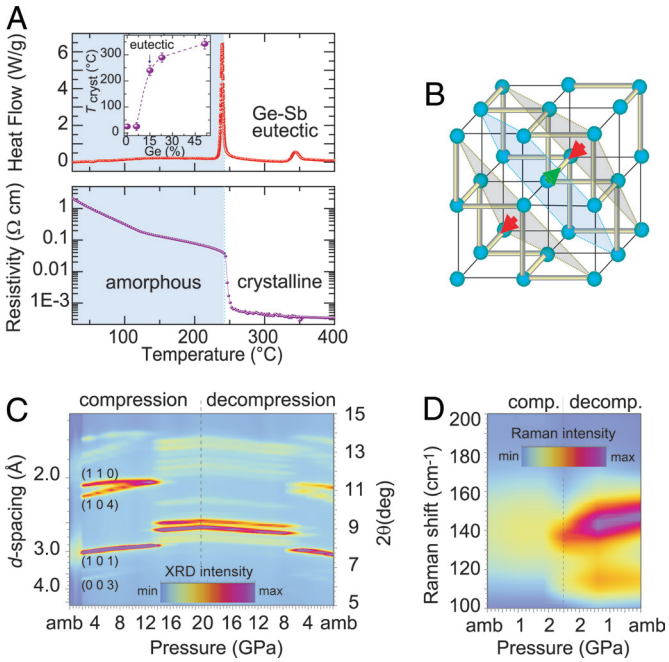


**Fig. 1.** Thermal and pressure crystallization of eutectic GeSb. (*A*) (*Upper*) Heat flow during a 10 °C/min temperature sweep shows the crystallization of a free-standing GeSb film obtained by liftoff. (*Lower*) Abrupt change in electrical resistivity during the phase change. (*B*) A7 Peierls distorted structure of GeSb formed from simple cubic structure by motion of atomic planes normal to (111) axis in alternate positive and negative senses. (*C*) Crystallization under pressure: X-ray diffraction spectra measured during compression/decompression cycle of initially amorphous GeSb to a maximum pressure of 21 GPa. The abrupt transition from the amorphous to the Peierls-distorted crystalline phase at 2 GPa is shown by the appearance of Bragg peaks. With increasing pressure, this distortion is removed (collapse of Bragg peak splitting at 14 GPa), followed immediately by a transition to the complex host–guest structure. (*D*) The amorphous–crystalline transformation monitored by Raman spectroscopy over a lower pressure range.

240 °C and has been demonstrated to amorphize by thermal quench in a fast-switching device configuration at the nanoscale (18). The structure of crystalline GeSb is shown by X-ray diffraction to be the same A7 structure as pure antimony [supporting information (SI) Fig. S1]. This structure is a distorted (16) simple cubic lattice with Ge randomly occupying Sb lattice sites. The nature of the distortion is that alternate planes of atoms transverse to the (111) (or equivalent) axis in the simple cubic structure displace in opposite directions along (111), resulting in a layered structure of closely spaced bilayers spaced apart relatively widely (Fig. 1*B*). The 6 equal nearest-neighbor bonds of the simple cubic structure are replaced by 3 short intrabilayer and 3 long interbilayer bonds. The distortion in Sb (also in Bi) is caused by an intimate coupling between the electronic structure and the lattice, the Peierls effect (21).

Our experiments demonstrate that under compressive load (decrease in volume) amorphous GeSb crystallizes, forming crystalline phases analogous to Sb (22, 23), which is known to crystallize explosively near room temperature (24). As shown in the X-ray diffraction data and Raman spectra under pressure (see *Materials and Methods*), crystallization (appearance of A7 structure Bragg peaks in Figs. 1*C* and Raman peaks in Fig. 1*D*) occurs at a threshold pressure of 2 GPa. The convergence of the (110) and (104) Bragg peaks seen in Fig. 1*C* indicates facile compression of the weak interbilayer bonds, relative to the stiffer intrabilayer bonds, resulting, at a pressure ≈13 GPa, in the disappearance of the Peierls distortion and formation of a simple cubic structure. At 14 Gpa, a further transition to a new intertwined tetragonal "host–guest" structure, also found in pure Sb (22), is observed. On decompression, the sequence of structures is reversed with some hysteresis, except that there is no return to the amorphous state. The amorphous sample has been irreversibly crystallized by cycling to above 2 GPa pressure—the hysteretic pressure–crystallization sequence being clearly confirmed in Raman spectroscopy (23); see Fig. S2.

We know that pure Sb (25) is a semimetal. So is GeSb, as witnessed by its relatively high resistivity in the metallic state, see Fig. 1. Indeed, it can be viewed as a Ge-doped Sb. This semimetallicity is the consequence of a Peierls distortion (1, 21, 26), driven by Fermi surface nesting in the nearly half-filled *p*-band, which underlies the simple cubic to A7 structural distortion. The distortion opens an incomplete energy gap—a "pseudogap"—at the Fermi level, lowering the total energy of the occupied electronic states and, hence, lowering the total electronic energy of the system (which "pays for" the elastic energy of the lattice distortion). Accordingly, in the crystalline phase, the measured metallic (Drude) conductivity (21) at low frequencies ($\omega \to 0$) is relatively high as clearly observed in the infrared (IR) conductivity data shown in Fig. 2*A*. In the crystalline phase, a partial gap in IR conductivity $\sigma(\omega)$—expected in the Peierls picture—at ≈0.5 eV is evident. In the amorphous phase, $\sigma(\omega)$ shows a full semiconducting gap of ≈1 eV.

Clearly, the (Peierls) band-gap mechanism with Fermi surface nesting no longer applies in the amorphous state (21) where long-range translational order is absent nor is there, at present, an analytically tractable theoretical model that can describe the phenomena. We handle this situation by means of AIMD, a technique that implements MD on a potential energy surface derived from solving the many-particle Schrödinger equation in the density functional approximation (12). AIMD (27) is used to closely examine the amorphous state reached in 2 ways. In one, the ensemble will be melted, followed by a rapid reduction in temperature (tens of picoseconds) (12). In the other, we will apply Le Chatelier's principle in reverse: Our new AIMD protocol will be used to amorphize GeSb by increasing the volume, equivalent to applying a tensile load.

Fig. 2*B* shows the AIMD-calculated optical conductivity $\sigma(\omega)$ of crystalline GeSb and of GeSb in the amorphous state, reached by both the thermal and volume methods. It is apparent that all basic experimental features of $\sigma(\omega)$ in both the amorphous and crystalline phase are reproduced. Note that the technique has the precision to correctly obtain both the frequency and conductivity scales to be in close correspondence with experiment [the density functional approach is known to underestimate energy gaps (14)]. We also note that optical conductivities of the amorphous state obtained under thermal- and under volume-quench conditions are essentially identical.

The correspondence of amorphous phases reached either by thermal or by nonthermal means is clearly evident in structural and bonding changes on the local level. Figs. 2 *C–E* compare the Ge coordination number and bond angle, for crystalline GeSb and for the 2 kinds of amorphized systems. In the crystalline phase (Fig. 2*C*), Ge tends to be 3-coordinated with nearly simple-cubic bond angles (i.e., it is substitutional in the A7 structure). In contrast, in both thermally (Fig. 2*D*) and volume-quenched (Fig. 2*E*) amorphous phases Ge is predominantly 4-coordinated with tetrahedral bond angles. We also find 4-coordinated Sb in the amorphous phases, but, instead of tetrahedral, they have incomplete trigonal-bipyramidal coordination. Our finding highlights the generality of 4-coordination in the amorphous state, the presence of which was previously found in the 225 compound (4). Indeed, this is unambigously confirmed in the bond transformation calculations (28) represented by Wannier functions in Fig. 2*F* for a 4-coordinated Ge site in the amorphous state. They show 4 equally strong, approximately

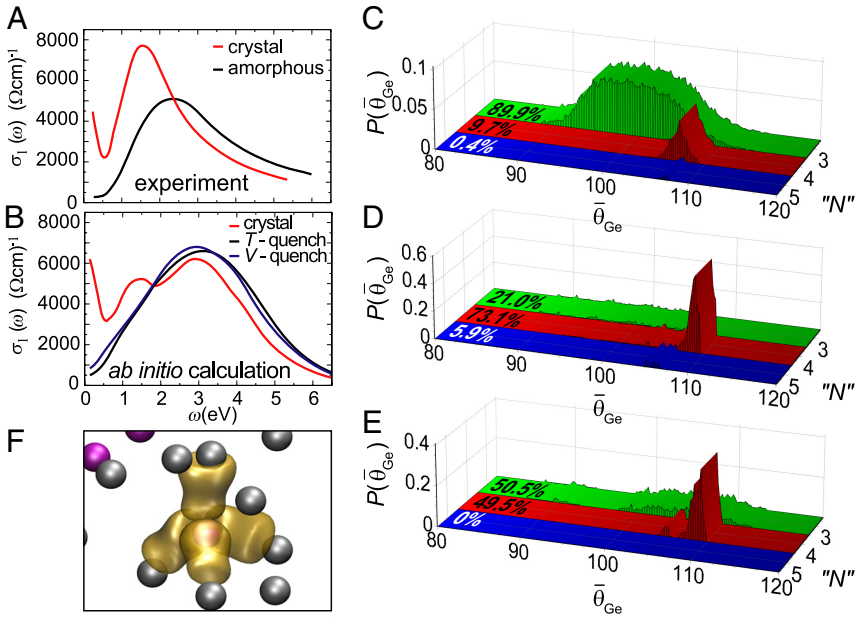


**Fig. 2.** Comparison of thermally and volume amorphized GeSb. (*A*) Measured infrared conductivity $\sigma(\omega)$ for GeSb crystal and amorphous films. (*B*) Optical conductivity $\sigma(\omega)$ computed by 192-atom AIMD for crystal, amorphous [thermally (T-) quenched in up to 25 ps], and amorphous [volume (V-) quenched in up to 50 ps]. (*C–E*) Probability distributions $P(\bar{\theta}_{Ge})$ of Sb-Ge-Sb bond angle $\bar{\theta}_{Ge}$ for different numbers ''*N*'' of Sb neighbors of Ge: crystal (*C*), amorphous (thermally quenched) (*D*), and amorphous (volume quenched) (*E*). (*F*) Wannier functions around a typical 4-coordinated Ge atom (magenta) in the volume-amorphized structure, showing the formation of 4 equivalent chemical bonds to Sb (gray), see *Results and Discussion*.

tetrahedral, chemical bonds, unlike the 3 strong and 3 weak bonds characteristic of the A7 structure.

Now we ask what drives the development of 4-coordination during the amorphization process (see Movie S1) and whether and how it connects with global order. We use the number of 4-coordinated sites as a metric of local order. We find that this local order parameter correlates closely with a global parameter, the total electronic energy $E_{tot}^{el}$. This is shown in Fig. 3*A* for volume amorphization, where a drop in $E_{tot}^{el}$ and the drop in the number of 3-coordinated Ge atoms ($P_3$) coincide. In Fig. 3*B*, the opening of a gap, as shown by the decreasing curvature $d^2N(E)/dE^2$ of the electronic density of states $N(E)$, and by the drop in (bulk) dc conductivity $\sigma(\omega = 0)$, develops in time along with the decrease in $P_3$. From the observed correlation between these 4 quantities, we conclude that amorphization is driven by a lowering of the electronic energy accompanying the opening of an energy gap in the electronic spectrum. Future simulations of the amorphization process, on much longer time scales, should access further details of gap opening by formation of interlayer bonds.

We arrive at the same conclusion by analyzing amorphization by quench from the melt. Fig. 3*C* shows 2 such amorphization runs at different cooling rates plotted as dc conductivity $\sigma(0)$ vs. total energy $E_{tot} = E_{tot}^{el} + E_s$, where $E_s$ represents lattice and electron–lattice interaction terms. In quenching from the melt, the system is lowering its global energy as it drops into a (metastable) locally accessible valley in the glassy energy landscape (9). Points of decreasing $E_{tot}$ represent points further along in the quench. What is remarkable, is that for both quench rates (and also for a single volume quench point) there is a seemingly "universal" relationship between $\sigma(0)$ and $E_{tot}$. We take decreasing $\sigma(0)$ as a measure of increasing semiconducting energy gap. Thus, $E_{tot}$ is lowered (becomes increasingly negative) as the energy gap increases. This is indeed expected and is consistent with the gap-driven picture, and it confirms our results for the volume amorphization in Fig. 3 *A* and *B*.

The electronic states in the neighborhood of the gap—as determined from their participation ratio (see Fig. S3)—are found to be poorly localized like typical band states, i.e., they cannot be associated with particular local-molecular rehybridization states. This supports the concept that phase change material amorphization follows a general scenario (exemplified in ref. 26) for structurally periodic systems), wherein a typically half-filled system can lower its electronic energy by any structural change, induced by electron–lattice coupling, which opens a gap between filled and empty states. The Peierls distortion mechanism, involving Fermi surface nesting, is just one example of this effect.

Now that we have established that the end state of the amorphization process is independent of the way it is reached, we note one unique and unusual feature of the volume-quench/volume expansion cycle: it is hysteretic. Fig. 4*A* summarizes the results of compressive (experiment) and tensile (simulation) stress applied to GeSb. Under compressive stress, at a threshold pressure ≈2 GPa, GeSb undergoes the amorphous-to-crystalline transformation (see Fig. 1*C*), whereas the reverse (crystalline-to-amorphous) transformation is found in AIMD to take place at a different threshold, approximately −2.5 GPa tensile load. The kinetics of this hysteretic process can be illustrated in a simple activation-energy picture of a free-energy diagram sketched in Fig. 4*B*. Upon applying positive pressure, the activation energy for crystallization is pulled down, so that the process can occur at room temperature. Conversely, the activation energy for amorphization is pulled down by expanding volume equivalent to applying negative pressure.

Our studies of amorphization demonstrate the presence of local structural changes—appearance of tetrahedrally bonded Ge and incomplete trigonal–bipyramidal bonded Sb (4)—distinguishing amorphization from crystallization. The absence of localization in near-gap states supports a gap-driven mechanism associated with the nearly half-filled *p*-band, where a gap separating filled and empty states forms by electron–lattice interaction, thus lowering the total electronic energy. The gap-driven mechanism suggests that similar amorphous states, characterized, e.g., by conductivity, reached by different paths (thermal or volume quench) should have similar energies, leading to

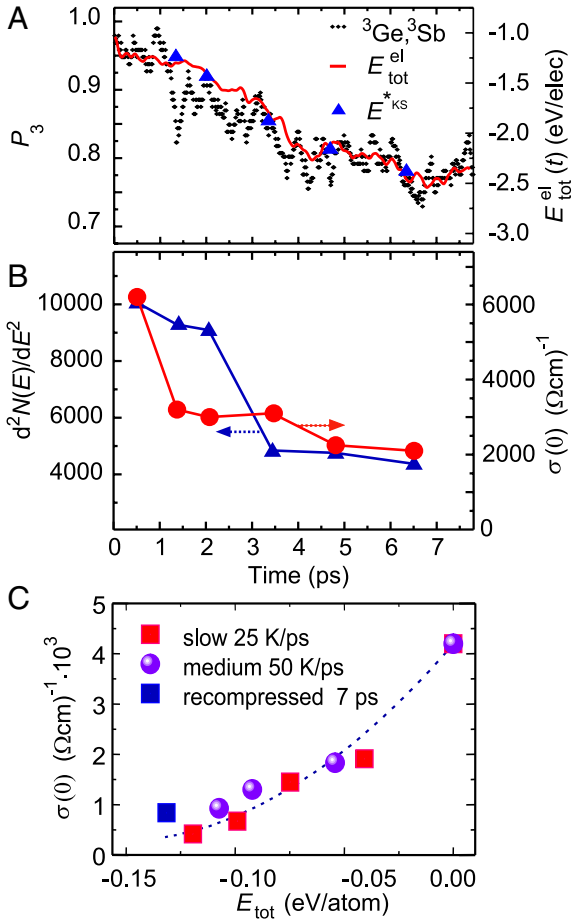


**Fig. 3.** Mechanism of the amorphization process. (*A* and *B*) Last 8 ps of volume amorphization run for 192 atom ensemble of eutectic GeSb under tensile load as a function of time. (*A*) A fraction $P^3$ of 3-coordinated atoms (which are replaced by 4-coordinated sites) and closely similar trend of total electronic energy $E^{el}_{tot}$ and scaled (×13) sum of the Kohn–Sham eigenenergies $E^*_{KS}$. (*B*) Curvature of gap $d^2N(E)/dE^2$ and zero-frequency electrical conductivity $\sigma(0)$, which show opening of gap in single-particle electron spectrum as amorphization proceeds. (*C*) During slow thermal quench, system drops into a local minimum in the glassy total-energy landscape. Graph shows how energy gap, measured inversely by zero frequency conductivity, tracks the total energy for several amorphization protocols. Red square (purple circle), thermal quench from 973 K to 300 K at average cooling rate 25 K/ps (50 K/ps). Blue square, 7-ps simulation of volume quenched sample after removal of tensile load.

plots such as Fig. 3*C*, potentially a previously undescribed way of classifying the phase change material glassy state. Further details of the scaling properties in Fig. 3*C* could be elucidated by means of a larger database of simulation runs in future work. Finally, we remark that the pressure-induced phase change and the corresponding hysteretic behavior are a consequence of GeSb being vacancy-free. Such behavior is expected in other phase-change materials in the "vacancy-free" class and can be envisioned as the operating principle of switching technology (29) requiring very low input power.

## Materials and Methods

**Experimental.** In this study, eutectic GeSb films (typically 100 nm thick) were deposited at room temperature, by using dc magnetron sputtering from a nominally Ge(15%):Sb(85%) target, onto either thermally oxidized (100) Si wafers for transport and optical temperature scans, or onto resist coated wafers, with subsequent lift-off to obtain free-standing films for calorimetry (see ref. 20 for details) and pressure studies. Raman studies were performed under isotropic compression, by using a symmetric piston-cylinder diamond anvil cell (DAC) equipped with 400-$\mu$m culet diamond anvils. The pressure was determined from the well-known pressure shift of the $R_1$ ruby fluorescence line (694.2 nm under ambient conditions) with an accuracy of ±0.05 GPa from ruby ($Cr^{+3}$-doped $\alpha$-$Al_2O_3$) chips placed inside the gasket sample chamber (see *SI Text*). The Raman spectra were collected in the range of 100–400 $cm^{-1}$, covering all of the significant Raman active modes of GeSb. X-ray diffraction spectra (at 30.55 keV; $\lambda$ = 0.4066 nm) were collected from GeSb in the same DAC at the high-energy, high-intensity superconducting-wiggler X-ray beam line X17C of the National Synchrotron Light Source at Brookhaven National Laboratory (see *SI Text*). Spectroscopic ellipsometry was used to obtain complex optical constants of amorphous (as deposited) and crystalline GeSb films on polished Si and (out-of-plane *c*-axis oriented) sapphire substrates. We used an ellipsometric setup attached to a Michelson interferometer (30) to collect data in infrared range 25 meV–1 eV; in visible-UV ranges, we used a standard rotating analyzer ellipsometer.

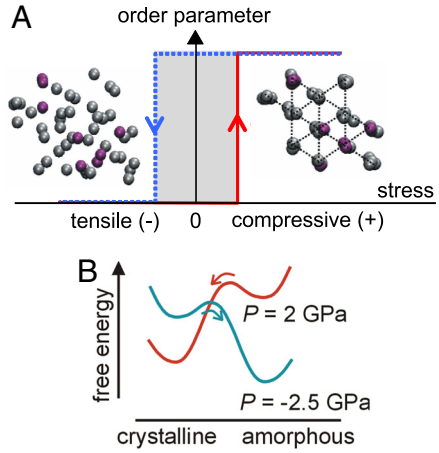


**Fig. 4.** Pressure-induced phase interconversion pathway in GeSb. (*A*) State vs. pressure diagram showing hysteresis, where upward vertical path is derived from diamond anvil experiments and downward vertical path from AIMD simulations. Frames from a 48-atom simulation of GeSb illustrate the amorphous and crystalline phases; dark gray, Sb, magenta, Ge. (*B*) A simple illustration of a global free-energy diagram. The 2 minima define the crystalline and amorphous states. Pressure bias flips the relative energy of the 2 wells: Compressive (+) pressure raises the amorphous state relative to the crystalline state, lowering the barrier to transition into the crystalline state. Tensile (−) pressure acts in reverse.

**Ab Initio MD.** The Car–Parrinello ab initio MD (12) studies presented herein were performed by using Kohn–Sham Density Functional Theory in conjunction with the B-LYP approximate density functional (31), and superscalable software and methods (27) on IBM's Blue Gene/L supercomputer. The computations were validated via extensive comparisons to previously published results (13, 14) and our own experimental datasets. The AIMD structure factors $S(Q)$ for the crystalline and amorphous phases agree closely with experiments (see Figs. S4 and S5).

**ACKNOWLEDGMENTS.** We acknowledge discussions with C. Lam, J. Crain, L. Kale, and their research groups, especially E. Bohm; computer time on Sharcnet and IBM Watson's Blue Gene/L supercomputer; the referees whose thoughtful comments helped improve the article; and the National Synchrotron Light Source (X17C), J. Hu and Z. Dong, for technical support and useful discussions. This work was supported by the Natural Sciences and Engineering Research Council (M.H.M.) and National Science Foundation Grant 0229959 (to G.J.M.).

1. Mott NF (1974) *Metal–Insulator Transitions* (Taylor & Francis, London).
2. Ovshinsky SR (1968) Reversible electrical switching phenomena in disordered structures. *Phys Rev Lett* 21:1450–1453.
3. Lankhorst MHR, Ketelaars BWSMM, Wolters RAM (2005) Low-cost and nanoscale non-volatile memory concept for future silicon chips. *Nat Mater* 4:347–352.
4. Kolobov AV, et al. (2004) Understanding the phase-change mechanism of rewritable optical media. *Nat Mater* 3:703–708.
5. Lencer D, et al. (2008) A map for phase-change materials. *Nat Mater* 7:972–977.
6. Klein A, et al. (2008) Changes in electronic structure and chemical bonding upon crystallization of the phase change material $GeSb_2Te_4$. *Phys Rev Lett* 100:016402.

7. Wełnic W, et al. (2006) Unraveling the interplay of local structure and physical properties in phase-change materials. *Nat Mater* 5:56–62.
8. van Pieterson L, Lankhorst MHR, van Schijndel M, Kulper AET, Roosen JHJ (2005) Phase-change recording materials with a growth-dominated crystallization mechanism: A materials overview. *J Appl Phys* 97:083520.
9. Angell CA (1991) Thermodynamic aspects of the glass transition in liquids and plastic crystals. *Pure Appl Chem* 63:1387–1392.
10. Pirovano A, Lacaita AL, Benvenuti A, Pellizzer F, Bez R (2004) Electronic switching in phase-change memories. *IEEE Trans Electron Devices* 51:452–459.
11. Greer AL, Mathur N (2000) Changing face of the chameleon. *Nature* 437:1246–1247.
12. Akola J, Jones RO (2008) Density functional study of amorphous, liquid and crystalline $Ge_2Sb_2Te_5$: Homopolar bonds and/or AB alternation? *J Phys Condens Matter* 20:465103.
13. Caravati S, Bernasconi M, Kühne TD, Krack M, Parrinello M (2007) Coexistence of tetrahedral- and octahedral-like sites in amorphous phase change materials. *Appl Phys Lett* 91:171906.
14. Bichara C, Johnson M, Raty JY (2005) Temperature-induced density anomaly in Te-rich liquid germanium tellurides: *p* versus $sp^3$ bonding? *Phys Rev Lett* 95:267801.
15. Sun Z, Zhou J, Ahuja R (2006) Structure of phase change materials for data storage. *Phys Rev Lett* 96:055507.
16. Raty JY, et al. (2002) Local structure of liquid GeTe via neutron scattering and ab initio simulations. *Phys Rev B* 65:115205.
17. Wüttig M, et al. (2007) The role of vacancies and local distortions in the design of new-phase-change materials. *Nat Mater* 6:122–128.
18. Chen YC, et al. (2006) Ultrathin phase-change bridge memory device using GeSb. *IEDM Tech Dig* 206:777–780.
19. Kolobov AV, et al. (2006) Pressure-induced site-selective disordering of $Ge_2Sb_2Te_5$: A new insight into phase-change optical recording. *Phys Rev Lett* 97:035701.
20. Cabral C, Jr, et al. (2008) Direct evidence for abrupt post-crystallization germ-anium precipitation in thin phase-change films of eutectic GeSb. *Appl Phys Lett* 93:071906.
21. Peierls RE (1956) *Quantum Theory of Solids* (Oxford Univ Press, Oxford).
22. Degtyareva O, McMahon MI, Nelmes RJ (2004) Pressure-induced incommensurate-to-incommensurate phase transition in antimony. *Phys Rev B* 70:184119.
23. Wang X, Kunc K, Loa I, Schwarz U, Syassen K (2006) Effect of pressure on the Raman modes of antimony. *Phys Rev B* 74:134305.
24. Wickersham CE, Bajor G, Greene JE (1978) Impulse stimulated 'explosive' crystallization of sputter deposited amorphous (In,Ga) Sb films. *Solid State Commun* 27:17–20.
25. Ormeci A, Rosner H (2004) Electronic structure and bonding in antimony and its high pressure phases. *Z Kristallogr* 219:370–375.
26. Johannes MD, Mazin II (2008) Fermi surface nesting and the origin of charge density waves in metals. *Phys Rev B* 77:165135.
27. Bohm E, et al. (2008) Fine grained parallelization of the Car–Parrinello ab-initio molecular dynamics method on the IBM BlueGene/L supercomputer. *IBM J Res Dev* 52:159–175.
28. Silvestrelli PL (1999) Maximally localized Wannier functions for simulations with supercells of general symmetry. *Phys Rev B* 59:9703–9706.
29. Elmegreen BG, et al. (2008) Piezo-driven non-volatile memory cell with hysteretic resistance. US patent application YOR920080512US1.
30. Qazilbash MM, et al. (2007) Mott transition in $VO_2$ revealed by infrared spectroscopy and nano-imaging. *Science* 318:1750–1753.
31. Becke AD (1988) Density-functional exchange-energy approximation with correct asymptotic behavior. *Phys Rev A* 38:3098.